Calibration Method for Multiple 2D LIDARs System

Mengwen He*, Huijing Zhao*, Jinshi Cui*, Hongbin Zha*

Abstract— Many robotic and mobile mapping systems have been developed using multiple 2D LIDARs (briefly multi-LIDAR system) to sense environment. In such systems, extrinsic calibration of all LIDARs is essential for making collaborative use of the data from different sensors. This research aims at developing a calibration method for multi-LIDAR systems at the general scene, such as an outdoor place or an underground parking-lot, without modification to environment by putting calibration targets. In this paper, the calibration method is proposed by aligning the 3D data of different LIDARs. They are concerned at two-levels: 1) reference calibration, i.e. finding the transformation from a reference LIDAR to the platform frame; 2) multi-LIDAR calibration, i.e. finding the LIDARs' relative geometries by referring to the reference one. The method is examined in calibrating the multiple 2D LIDARs on an intelligent vehicle platform POSS-V, where the data collected through a driving in an underground parking-lot are registered to find sensors' geometry. Calibration accuracy is examined by comparing with a CAD model of the scene, which was measured by using a total station.

I. INTRODUCTION

Nowadays, 2D LIDAR sensors, such as SICK LMS, Hokuyo URG and UTM, have been widely exploited in robotics and mobile mapping platforms for 3D modeling [1], [2], SLAM (Simultaneous Localization and Mapping)[3], object detection [4], [5], [6], autonomous navagation [7], [8] etc. As a 2D LIDAR sensor profiles at the environment on only a certain plane, in order to acquire more complete knowledge to the robot's surroundings, some sensing systems [9], [10] have been developed using a number of 2D LIDARs that possess much different viewpoints and scanning planes (referred to as the multi-LIDAR system). In such systems, LIDAR sensors need to be well calibrated so as to integrate the data of different sensors to a global coordinate system, and make collaborative use of them.

Calibration of multi-LIDAR system (more specifically, extrinsic calibration) is often poorly documented. Among the documented works, there are generally two types of calibration: 1) calibrating a LIDAR to a reference frame defined by such as a camera [11], [12], [13] or the ego-vehicles odometry center [14] or 2) finding the relative geometries among different LIDARs [15], [16]. These calibration methods usually require some modification of the scene by introducing landmarks that are visible (or detectable) by LIDARs, such as specifically placed reflective targets [15], poles [17], checker boards [18], which introduce laborious

*M. He, H. Zhao, J. Cui and H. Zhao are with the State Key Lab of Machine Perception (MOE), School of EECS, Peking University, Beijing, P.R. China alexanderhmw at pku.edu.cn
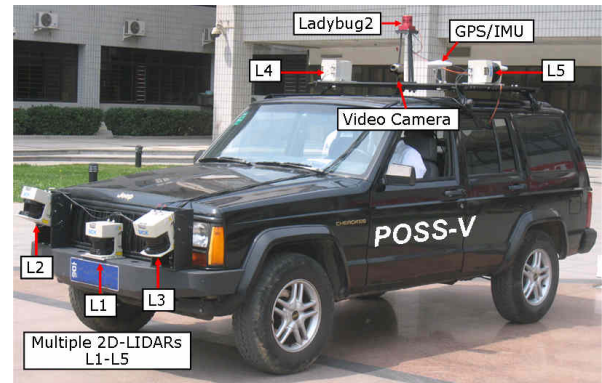
Fig. 1. The POSS-V platform that is used to study the calibration of a multiple 2D LIDAR system.

field work, or rely on special facilities [16]. Furthermore, some methods make use of the visible laser [19] or require that the LIDAR can measure reflectivity [15], which put strong restriction to the adaptiveness of the methods on a broad range of systems. Calibration of a 3D LIDAR system that possesses multiple laser beams has also been studied [16], [20]. As their methods put some assumptions to the scene, such as contiguous surfaces, further elaborations are required to adapt the methods to a more general scene. In a multi-LIDAR system, the scanning planes and viewpoints of 2D LIDARs could be greatly different, yielding much occlusions between the data of different sensors, and making it a big challenge in generating data correspondences. Thus issues are not well studied in literature.

This research studies the calibration method of a multi-LIDAR system, where a number of 2D LIDARs are rigidly mounted on a robotic platform at different locations and directions. The experimental platform used in this research is shown in Fig.1. However the method developed is not restricted to such a system, as a more general purpose method is aimed. A two-level calibration method is concerned, which find 1) the transformation from a reference LIDAR to the platform frame, which is usually defined by the localization module, and 2) the geometric relationships between the reference LIDAR and other LIDARs. We aim at calibration in a general urban environment, such as an outdoor place or a parking-lot, without any modification of the environment nor requiring special facilities. In the authors previous work [21], a pairwise calibration method that finds the relative geometry between two LIDARs was proposed. This paper is an extension of the previous work, where novel contributions are 1) a method that calibrating a reference LIDAR to the platform, and 2) a method that simultaneously calibrating
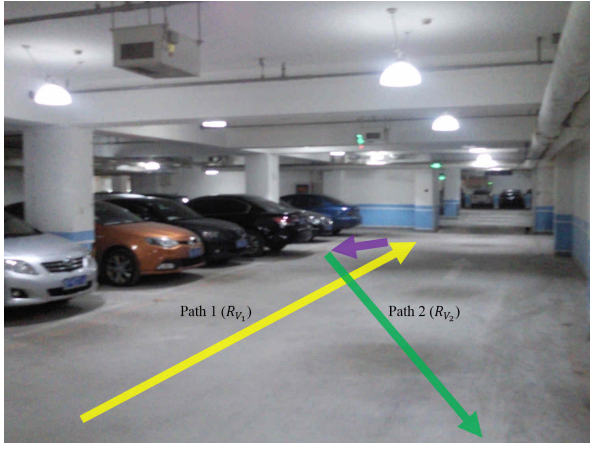
Fig. 2. The underground parking lot in our experiment. The yellow and green lines are the designed V-shape pathes.

multi-LIDAR with the help of a well-calibrated reference LIDAR in global level.

An experiment was conducted in an underground parking-lot. where $L4$ in Fig.1 is selected as the reference one, $L2$ and $L3$ are calibrated with $L4$ to achieve a more complete and consistent LIDAR sensing to the environment. LIDAR data are collected by driving the platform along a V-shape path (as shown in Fig.2), which is theoretically proved in section 3, and demonstrated efficient in experiment. Geometric features (e.g. the planes in parking lot scene) are extracted from the 3D point-clouds of each LIDAR, and are aligned to find a geometric transformation from the reference LIDAR (i.e. $L4$ in Fig.1) to the platform frame, and from the other LIDARs (i.e. $L2$, $L3$ in Fig.1) to the reference one. The underground parking lot was measured using a total station to find a 3D model of the environment as the ground truth, which are used to evaluate the calibration accuracy by comparing the integrated LIDAR data with the 3D model. We drove the platform to collect data for test along a C-curve path at the corner of the parking-lot (Fig.6). The C-curve is different with the V-shape, because it has no straight path, and the straight path is a requirement for our calibration method. So using the data collected on the C-curve path to test our calibration result obtained on the V-shape path is complete and reliable.

Below we give an overview to the calibration method in section 2, present the methods of the reference LIDAR calibration and the multiple LIDARs calibration in section 3 and 4 respectively, and address the experimental results at section 5, followed by conclusion and future work at section 6.

II. CALIBRATION METHOD OVERVIEW

The calibration method for multi-LIDAR system is to calculate each LIDAR's extrinsic calibration parameters, which contain the LIDAR's rotation and translation in the platform's coordinate. In this paper, we notate the LIDAR's calibration parameters as a transformation matrix M_L, then notate the rotation term as matrix R_L and the translation

term as vector $\mathbf{T}_L$. The rotation matrix in this paper is parameterized using Euler angles.

With the localization data of the platform, we can generate the 3D world point-cloud $\{\mathbf{p}^i\}$ of the scanned area from the 2D local point-data $\{\mathbf{q}^i\}$ collected by the LIDAR. If we notate the localization data as a series of transformation matrices $\{M_V{}^i\}$ corresponds to the 2D point-data $\{\mathbf{q}^i\}$, then the generation of 3D point-cloud is as Eq.1.

$$\mathbf{p}^i = M_V{}^i \cdot M_L \cdot \mathbf{q}^i \qquad (1)$$

But in reality, we always use the estimated LIDAR's calibration parameters to generate the 3D point-cloud. In this paper, we notate the LIDAR's estimated calibration parameters as the estimated matrix $\hat{M}_L$ of M_L, then notate the estimated rotation term as $\hat{R}_L$ and the estimated translation term as $\hat{\mathbf{T}}_L$. The estimated LIDAR's calibration parameters must contain calibration error, which will deviate the true 3D point-cloud $\{\mathbf{p}^i\}$ to the estimated 3D point-cloud $\{\hat{\mathbf{p}}^i\}$ (Eq.2). The calibration error is regarded as a error transformation M_e to connect $\hat{M}_L$ and M_L as Eq.3, then notate its rotation term as R_e and translation term as $\mathbf{T}_e$.

$$\hat{\mathbf{p}}^i = M_V{}^i \cdot \hat{M}_L \cdot \mathbf{q}^i \qquad (2)$$

$$\hat{M}_L = M_e \cdot M_L \qquad (3)$$

In our research, we calibrate the LIDARs by minimizing its calibration error (making $M_e \to I$), which means the estimated calibration parameters $\hat{M}_L \to M_L$, as well as the alignment between $\{\hat{\mathbf{p}}^i\}$ and $\{\mathbf{p}^i\}$. But to directly minimize the unknown calibration error is difficult, so our strategy is to minimize a strongly related objective function, which is the alignment distance between the generated 3D point-clouds, by tuning the estimated calibration parameters $\hat{M}_L$.

Our calibration method for multi-LIDAR system is divided into two sequential stages: reference and multiple LIDARs calibration. The reference calibration chooses one LIDAR as reference for other LIDAR's calibration and then calibrates it to the platform frame. After reference calibration, the multiple LIDARs calibration calibrates the other target LIDARs with the help of the reference. Finally all the LIDARs are properly calibrated to the platform frame. These two stages are almost same except the composition of the optimization formula for minimizing the alignment distance between 3D point-clouds (will be discussed in section 3 and 4).

In this research, we refer to the author's previous work [21] and use the distance between multi-type geometric features to represent the alignment distance between 3D point-clouds. The geometric feature G is defined as Eq.4, where $\{\mathbf{p}_k\}$ is the feature's 3D points; ϕ, f^ϕ are the geometric type and formula (in this paper, we only use plane features, which is the only available features in the underground parking-lot); $\{\mu, \sigma^2\}$ is the feature's reliability measurement. The distance $D_G(G_1, G_2)$ between the features G_1 and G_2 is defined as Eq.5.

$$G = \{\{\mathbf{p}^k\}, \phi = \text{plane}, f^\phi, \{\mu, \sigma^2\}\} \quad (4)$$

$$D_G(G_1, G_2) = \sum_i \frac{(f_1^\phi(\mathbf{p}_2^i) - \mu_1)^2}{\sigma_1^2} \quad (5)$$

The minimized distance between two sets of geometric feature is obtained by tuning estimated calibration parameters $\hat{M}_L$, which will regenerate the 3D point-cloud P as well as its geometric features $\{G^j\}$. For convenience we define a function for the geometric feature regeneration as Eq.6, a sum of geometric feature distances between two 3D point-clouds P_1 and P_2 as Eq.7, and an expression of the relationship between a regenerated 3D point-cloud P and its new geometric features $\{G^j\}$ caused by tuning the estimated calibration parameters $\hat{M}_L$ as Eq.8. In [21], the author had demonstrated the accuracy and robustness of the alignment of geometry features in 3D point-clouds.

$$G(\hat{M}_L) = \{\{\mathbf{p}^k\}(\hat{M}_L), \phi, f^\phi(\hat{M}_L), \{\mu, \sigma^2\}(\hat{M}_L)\} \quad (6)$$

$$D_P(P_1, P_2) = \sum_j D_G(G_1^j, G_2^j) \quad (7)$$

$$P(\hat{M}_L) \Rightarrow \{G^j(\hat{M}_L)\} \quad (8)$$

III. REFERENCE LIDAR CALIBRATION

The reference LIDAR calibration stage is to choose a LIDAR as a reference for other LIDARs' calibration and then calibrate it to the platform frame. In our research, we calibrate the reference LIDAR without requiring any measured calibration targets, but only by aligning 3D point-clouds generated by the reference LIDAR.

A. Reference LIDAR Calibration Method

If we drive the platform in two different directions to collect two 3D point-clouds of a scene, say P_1 and P_2, by using a reference LIDAR in the same configuration. The existence of calibration error will make these two 3D point-clouds misaligned. Thus our strategy for the reference LIDAR calibration is to align these two 3D point-clouds to eliminate the calibration error. So the optimization formula for the alignment of P_1 and P_2 using their geometric features is defined as Eq.9.

$$\begin{aligned} \hat{M}_L^* &= arg\min_{\hat{M}_L} D_P(P_1(\hat{M}_L), P_2(\hat{M}_L)) \\ &= arg\min_{\hat{M}_L} \sum_j D_G(G_1^j(\hat{M}_L), G_2^j(\hat{M}_L)) \end{aligned} \quad (9)$$

In our experiment, we use 2D SLAM for localization. In order to guarantee the localizations are in the same frame, we continuously drove the platform along a V-shape path (Fig.2). In generated 3D point-clouds P_1 and P_2, we manually extracted the matched plane features for alignment. Then we minimize the objective function defined in Eq.9 for the reference LIDAR calibration (the detail of the optimization process refers to [21]). The tuned variables are 3 rotation

angles and 3 translation values of estimated calibration parameters. Finally after alignment, if there is no mirror reflection occurs, then the calibration error is eliminated in theory. But we only use 2D SLAM for localization, so the calibration translation error on Z-axis cannot be eliminated, we just used a measured value for instead. This only influences the absolute height of LIDARs in the final calibration results but the relative height can still be hold.

B. Reference LIDAR Calibration Theory

The author's previous work [21] has demonstrated that if the platform drives straightly, then the calibration error M_e will generate an invertible affine transformation M_A from the true 3D points $\{\mathbf{p}^i\}$ to the estimated 3D points $\{\hat{\mathbf{p}}^i\}$ (Eq.10). This deviation transformation is decided by three factors: the normal of the LIDAR's scan plane in the platform frame $\mathbf{n}$, the calibration error M_e and the direction of the straight driving R_V.

$$\hat{\mathbf{p}}^i = M_A(\mathbf{n}, M_e, R_V) \cdot \tilde{\mathbf{p}}^i \quad (10)$$

Assume there are two 3D point-clouds P_1 and P_2, which are collected by the reference LIDAR on two pathes with different directions $R_{V1} \neq R_{V2}$, then there are two deviation transformation matrices M_{A1} and M_{A2}. If the P_1 and P_2 are aligned, then $M_{A1} = M_{A2}$. In Appendix A, we have demonstrated that if $M_{A1} = M_{A2}$, the calibration error will be eliminated ($M_e = I$).

IV. MULTIPLE LIDARs CALIBRATION

After reference LIDAR calibration, the multiple LIDARs calibration stage is to simultaneously calibrate other target LIDARs to the platform frame with the help of reference LIDAR. In our research, we calibrate target LIDARs by aligning their 3D point-clouds to the constant 3D point-cloud of the reference LIDAR. In order to improve the result in global level, the alignment among the 3D point-clouds of the target LIDARs is also concerned.

A. Multiple LIDARs Calibration Method

The existence of the calibration error of one target LIDAR L_t will make its generated 3D point-cloud P_t misaligned to the constant 3D point-cloud P_r of the reference LIDAR L_r. So our strategy for calibrating one target LIDAR is to align the 3D point-cloud P_t to the 3D point-cloud P_r to make their calibration errors are in the same level. So the optimization formula for the alignment of P_t and P_r using their geometric features is defined as Eq.11, which is referred to as pairwise LIDARs calibration. We can combine all the pairwise calibration to do simultaneous optimization as Eq.12, which is referred to as multiple LIDARs calibration

$$\begin{aligned} \hat{M}_{L_t}^* &= arg\min_{\hat{M}_{L_t}} D_P(P_r, P_t(\hat{M}_{L_t})) \\ &= arg\min_{\hat{M}_{L_t}} \sum_j D_G(G_r^j, G_t^j(\hat{M}_{L_t})) \end{aligned} \quad (11)$$

$$\{\hat{M}_{L_t}^{k*}\} = arg\min_{\{\hat{M}_{L_t}^k\}} \sum_k D_P(P_r, P_t^k(\hat{M}_{L_t}^k)) \quad (12)$$

But this optimization performs bad in global level, which is manifested in the misalignment of 3D point-clouds generated by the target LIDARs. So the optimization formula for the alignment among target LIDARs' 3D point-clouds, defined as Eq.13, is added to Eq.12 to perform global optimization.

$$\{\hat{M}_{L_t}^{k*}\} = arg \min_{\{\hat{M}_{L_t}^k\}} \sum_{l \neq m} D_P(P_t^l(\hat{M}_{L_t}^l), P_t^m(\hat{M}_{L_t}^m)) \quad (13)$$

In our experiment, we simultaneously used all LIDARs to collect the data on the same straight path. In the generated 3D point-clouds, we manually extracted the plane features and minimize the objective function Eq.12+Eq.13 for multiple LIDARs calibration . Assume there are n target LIDARs, the tuned variables are $3 \times n$ rotation angles and $3 \times n$ translation values of the estimated calibration parameters. Finally after alignment, the calibration errors of the target LIDARs are in the same level with the reference LIDAR.

B. Multiple LIDARs Calibration Theory

For the first term of the optimization formula for multiple LIDARs calibration in Eq.12, assume there are two 3D point-clouds P_r and P_t, which are collect by the well-calibrated reference LIDAR and the target LIDAR on the same path, then according to Eq.10, there are two deviation transformation matrices M_{A_r} and M_{A_t}. If the P_r and P_t are aligned, then $M_{A_r} = M_{A_t}$. In Appendix B, we have demonstrated that if $M_{A_r} = M_{A_t}$, the calibration error will be eliminated $M_{e_t} = M_{e_r} = I$.

For the second term of the optimization formula for multiple LIDARs calibration in Eq.13, it is a punishment term that compensates the first term. Because the reference LIDAR's 3D point-cloud cannot cover all the space around the platform, the first term cannot work well in its uncovered space. The second term concerns the alignment in the reference's uncovered space, then the calibration error will be reduced in the global level.

V. EXPERIMENT RESULT

The vehicle platform POSS-V (Fig.1) was used in this research to evaluate the calibration method for a multi-LIDAR system. An experiment was conducted by using the data collected through a driving along a V-shape path (Fig.2), where the L_4, scanning vertically to the right of the vehicle, is regarded as the reference LIDAR; the L_2, scanning upward to the ahead ceiling surface, and L_3, scanning downward to the ahead road surface, are calibrated with platform by referring to L_4. As the experiment was conducted at a flat underground parking lot, the horizontal LIDAR, i.e. L_1, was used to perform localization through a LIDAR-based 2D SLAM (Fig.3), and its frame is regarded as that of the platform.

Below we present the experimental results in reference and multi-LIDAR calibrations, which are conducted by aligning the plane features of the 3D points from each LIDAR. We manually set seeds for region-grow based planes extraction
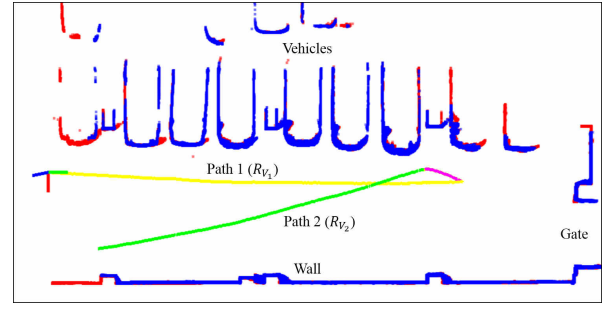

Fig. 3. The SLAM result of the designed V-shape path in the underground parking lot.
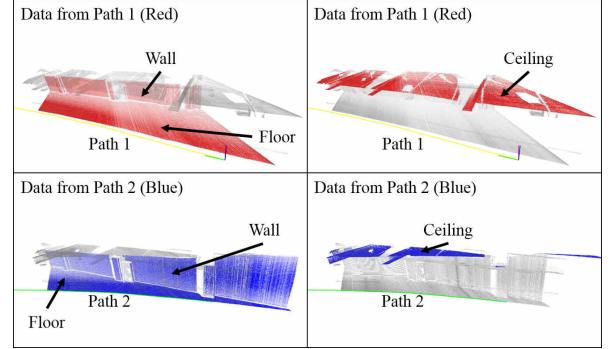

Fig. 4. The 3D point-clouds of Path 1 and 2. The floor, wall and ceiling parts are separately present as highlight for clear viewing.

and selected a coarse calibration parameters as initial value. We evaluated the result's accuracy by comparing the sensing results to the measured 3D scene model from a total station.

A. Reference LIDAR calibration

The data for reference LIDAR calibration was collected by driving the platform along the V-shape path. The 3D point-clouds and their plane features are shown in Fig.4. After alignment, we can get aligned 3D point-clouds, shown in Fig.5. According to the reference LIDAR calibration theory, if the 3D point-clouds are aligned and there is no mirror reflection occurs, the calibration error is eliminated except the translation error along the Z-axis.

In order to demonstrate the reference LIDAR calibration result is acceptable, we test the result in the test area shown in Fig.6, which is a corner of the underground parking-lot. We used a total station to build a CAD model of the test area and special focus is cast on the planes' direction in this scene. And we drove the platform along a C-curve path to test whether the generated 3D point-cloud is consistent with the measured CAD model. The SLAM result and the generated 3D point-cloud are shown in Fig. 6. The numerical analysis of the calibration result is to calculate the angles between extracted planes in the 3D point-cloud and the result is shown in Table.I. Take the table's first row for example, the angle between the Wall1 and Wall2 (Fig.6) is calculated by the angle between the normal vectors of the Wall1 and Wall2.

From Table.I, the most improvement is the angle between two vertical walls (Wall1 and Wall2, $86.6127° \rightarrow 89.9894°$),
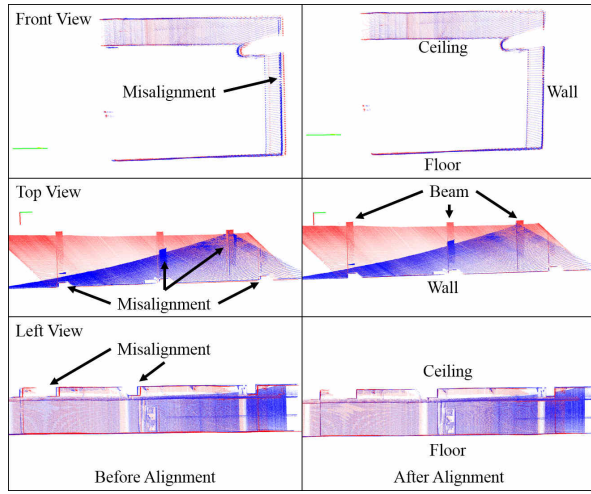
Fig. 5. Alignment of the 3D point-clouds in 3 viewpoints. The red 3D point-cloud is from path 1 and the blue 3D point-cloud is from path 2. Left is before alignment and right is after alignment.
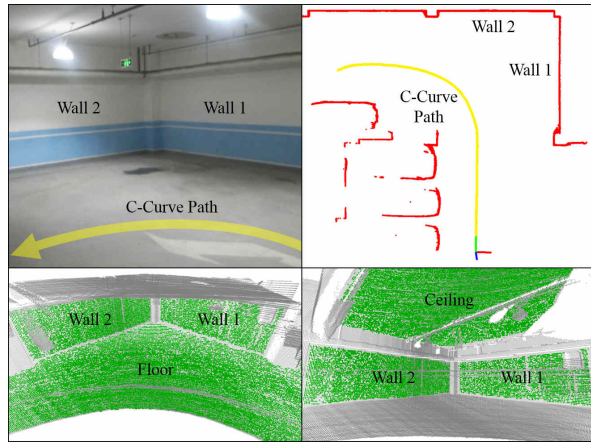

Fig. 6. Upper left:the test area. Upper right: the SLAM result. Lower: the generated 3D point-cloud from L_4. The green planes are used to test the calibration result.

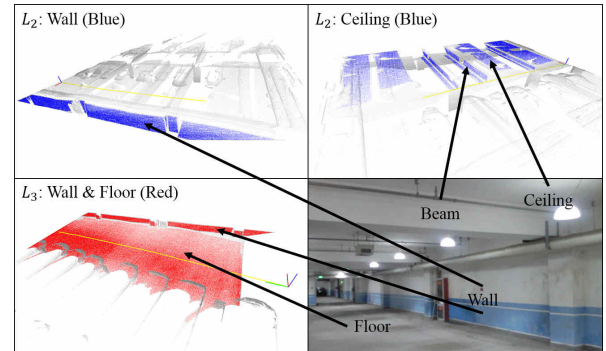| Planes Angle	Before Calibration(°)	After Calibration(°)	Ground-truth(°)	Eval. (Δ Change)
Wall1 Wall2	86.6127 (Δ = 3.3349)	89.9894 (Δ = 0.0418)	89.9476	Excellent (↓↓↓)
Ceiling Floor	0.7385 (Δ = 0.6700)	0.4955 (Δ = 0.4270)	0.0685	Good (↓)
Ceiling Wall1	88.8720 (Δ = 1.0559)	89.7993 (Δ = 0.1286)	89.9279	Excellent (↓↓)
Ceiling Wall2	89.9643 (Δ = 0.1263)	89.9606 (Δ = 0.1226)	89.8380	Excellent (↓)
Floor Wall1	89.3787 (Δ = 0.4882)	89.4310 (Δ = 0.4359)	89.8669	Good (↓)
Floor Wall2	89.8134 (Δ = 0.0064)	89.4050 (Δ = 0.4020)	89.8070	Good (↑)

Fig. 7. The 3D point-clouds and their plane features for multiple LIDARs calibration.

terms. The features from target LIDARs L_2 and L_3 for the second optimization term Eq.13 are shown in Fig.9. After alignment, shown in Fig.10, the alignment result around the vehicle side improved.

Finally we compared these two calibration results to the ground-truth to demonstrate that 1) the second optimization term Eq.13 in multiple LIDARs calibration optimization formula improves the result in the global level, and 2) the multiple LIDARs calibration result is acceptable.

The first demonstration is conducted by testing the angle between the ceiling plane from the LIDAR L_2 and the floor plane from the LIDAR L_3 in the calibration area shown in Fig.7 and the numerical result is shown in Table.II. We found that with the second optimization term Eq.13, the calibration error changes from 1.2390 to 1.0465 and gets closer to the reference LIDAR's calibration error 0.9403. With the Fig.8 and the Fig.10, we demonstrated that the second optimization term Eq.13 improves the calibration result in the global level.

The second demonstration is conducted by testing the angles between planes from the LIDARs L_2 and L_3 in the test area shown in Fig.6. The Fig.11 shows the 3D point-clouds of L_2 and L_3 in the test area and the Fig.12 shows the alignment of these 3D point-clouds. The numerical analysis is shown in Table.III. The column of error gap is the difference between the multiple calibration result and the reference calibration result, and it is an index to show

which indicates that the initial calibration parameters are bad in rotation around Z-axis. Except the result between the Floor and Wall2 (last row in Table.I), the rest errors of calibration result are reduced. The difference between the ground-truth and the calibrated 3D point-cloud is no more than 0.4 degree. Taking localization error, sensing error of LIDAR and measurement error of ground-truth into account, the reference LIDAR calibration result is acceptable.

B. Multiple LIDARs calibration

Firstly we calibrated the LIDARs L_2 and L_3 in the absence of the second optimization term Eq.13. Fig.7 shows the extracted features, whose 3D points are collected on the path 1 in Fig.2, for the first optimization term Eq.12. After alignment, shown in Fig.8, the alignment result around the wall side, where the features are extracted, is acceptable, but the alignment result around the vehicle side is bad, which is manifested in the misalignment of 3D point-clouds.

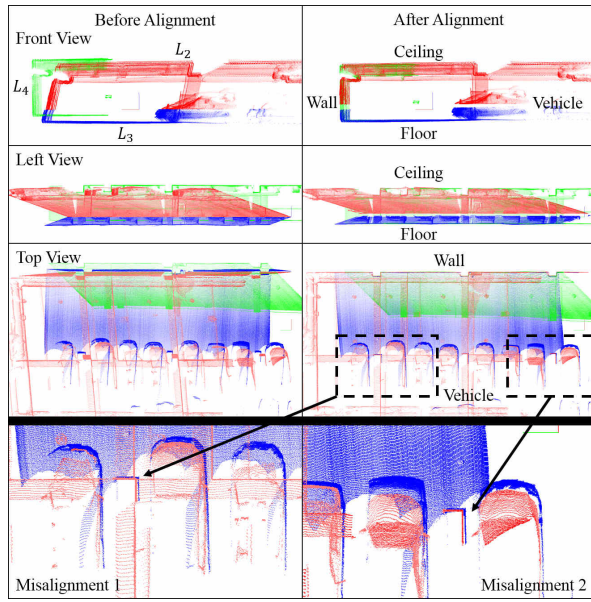Then we calibrated the LIDARs using both optimization

Fig. 8. The alignment results of multiple LIDARs calibration without the second optimization term Eq.13. The green 3D point-cloud is from the reference LIDAR L_4, the blue and the red ones are from the target LIDARs L_2 and L_3. The last row shows the misalignment.
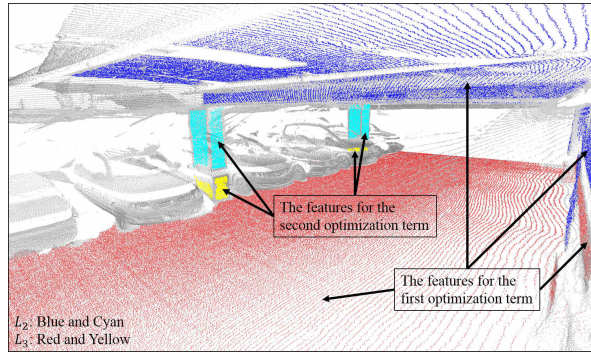

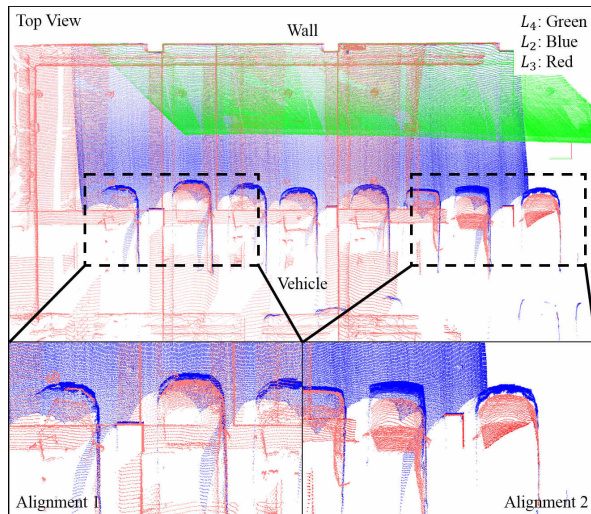Fig. 9. All the plane features for multiple LIDARs calibration using both optimization terms.

Fig. 10. The alignment result of multiple LIDARs calibration with the second optimization term Eq.13. The color is same with Fig.8. The last row shows the improvement in the global level.

TABLE II
EFFICIENCY OF EQ.13 IN CALIBRATION AREA (FIG.7)

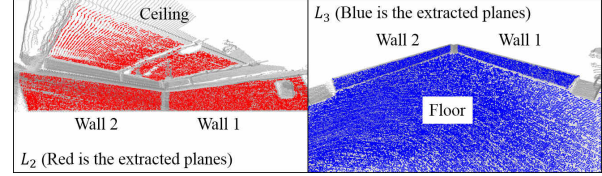| Angle Between Two Planes	Without Eq.13	With Eq.13	Reference Result	Ground-truth
Ceiling(L_2)-Floor(L_3)	1.2390°	1.0465°	0.9403°	0.0453°

Fig. 11. 3D point-clouds of L_2 and L_3 in the test area. Highlighted parts are the extracted planes for testing.

the difference of the calibration error level. Form Table.III, the difference between the reference LIDAR calibration error and the target LIDARs calibration errors is no more than 0.5 degree, so the multiple LIDARs calibration result is in the same level with the reference LIDAR and is also acceptable.

The straight pathes are required in calibration theory, but in reality, a lightly curved path can be seen as straight in a short path segment. The demonstration of the calibration method on a curved path is our next work.

VI. CONCLUSION

The research proposed a calibration method for multi-LIDAR systems, which is conducted in general environment, without modification to the environment by such as putting targets, nor relying on special facilities. The calibration method is divided into two sequential stages: 1) reference calibration, i.e. finding the transformation from a reference LIDAR to the platform frame; 2) multi-LIDAR calibration, i.e. find the LIDARs' relative geometries by referring to the reference one. After the platform's driving along a V-shape path, which has been theoretically proved in this paper and demonstrated efficient in experiment, the data of each sensor are aligned using their geometric features to find the transformations from the reference LIDAR to the platform and from other LIDARs to the reference one. Efficiency and
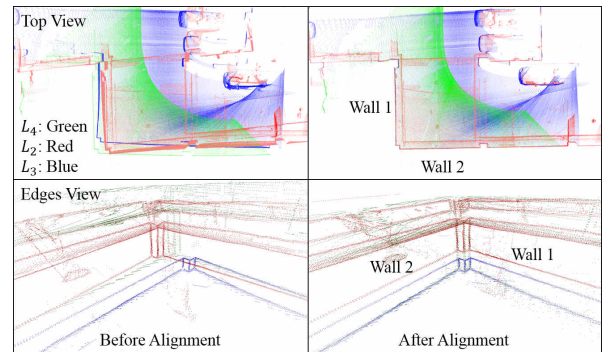

Fig. 12. Left: before calibration. Right: after calibration. The edges view shows the DoN (Difference of Normal) features.

TABLE III

MULTIPLE LIDARs CALIBRATION RESULT IN TEST AREA (FIG.12)

Angle Between Two Planes	Multiple Result	Reference Result	Ground-truth	Error Gap
Ceiling-Floor	0.8786°	0.4955°	0.0685°	0.3831°
Wall1(L_2)-Wall1(L_3)	0.3866°	-	-	0.3866°
Wall2(L_2)-Wall2(L_3)	0.5045°	-	-	0.5045°
Ceiling-Wall1(L_2)	89.5609°	89.7993°	89.9279°	0.2384°
Floor-Wall1(L_3)	89.5176°	89.4310°	89.8669°	0.0866°
Ceiling-Wall2(L_2)	89.7607°	89.9606°	89.8380°	0.1999°
Floor-Wall2(L_3)	89.4806°	89.4050°	89.8070°	0.0756°

TABLE IV

NOTATIONS

Var.	Comment
M_A	deviation transformation from true point to estimated point
R_A	linear map matrix term of M_A
$\mathbf{T}_A$	translation term of M_A
$M_V{}^i$	platform's transformation at time i in the world frame
$R_V{}^i$	rotation term of $M_V{}^i$
R_V	platform drives straightly ($R_V{}^i = R_V$)
$\mathbf{T}_V{}^i$	translation term of $M_V{}^i$
M_L	geometric transformation of the LIDAR in the vehicle frame
R_L	rotation term of M_L
$\mathbf{T}_L$	translation term of M_L
M_e	calibration error transformation
R_e	rotation term of M_e
$\mathbf{T}_e$	translation term of M_e
$\hat{M}_L$	estimated M_L, $\hat{M}_L = M_e \cdot M_L$
$\hat{R}_L$	rotation term of $\hat{M}_L$
$\hat{\mathbf{T}}_L$	translation term of $\hat{M}_L$
$\mathbf{t}$	vehicle forward direction in the vehicle frame ($(0,1,0)^T$)
$\mathbf{n}$	LIDAR scan plane's normal in the vehicle frame ($(\alpha,\beta,\gamma)^T$)
$\beta \neq 0$	requirement of invertible affine deviation transformation.
$\mathbf{O}_L{}^i$	position of the LIDAR's origin in the world frame at time i

accuracy has been demonstrated through an experiment at an underground parking-lot in Peking University. Future work will address on an automated feature extraction and selection algorithm, which is a basis in extending the method to an online based calibration.

VII. APPENDIX

A. Reference LIDAR Calibration Theory Derivation

The detailed deviation transformation M_A in Eq.10 is as Eq.14. The detailed notations are listed in Table.IV.

$$M_A = \begin{bmatrix} R_A & \mathbf{T}_A \\ \mathbf{0} & 1 \end{bmatrix}, M_e = \begin{bmatrix} R_e & \mathbf{T}_e \\ \mathbf{0} & 1 \end{bmatrix} \quad (14)$$

$$\text{where} \begin{cases} R_A &= E + (I-E) \cdot J \\ \mathbf{T}_A &= \mathbf{T}_V^0 - R_A \cdot \mathbf{O}_L^0 + R_V \cdot \hat{\mathbf{T}}_L \\ E &= R_V \cdot R_e \cdot R_V^T \\ J &= R_V \cdot \frac{\mathbf{t} \cdot \mathbf{n}^T}{\mathbf{n}^T \cdot \mathbf{t}} \cdot R_V^T \\ \hat{\mathbf{T}}_L &= R_e \cdot \mathbf{T}_L + \mathbf{T}_e \end{cases}$$

For the two 3D point-clouds P_1 and P_2 mentioned in section 3, there are two deviation transformations M_{A1} and

M_{A2}. If $M_{A1} = M_{A2}$ then P_1 and P_2 are aligned. If P_1 and P_2 are aligned and each contains more than 4 non-deteriorate points, then $M_{A1} = M_{A2}$. If we assume the rotation axis of R_V is Z-axis, then we demonstrated that if $R_{A1} = R_{A2} = R'_A$ holds, there are only two solutions for R'_A and R_e:

$$\text{Solution 1} \begin{cases} R'_A &= I \\ R_e &= I \end{cases}$$

$$\text{Solution 2} \begin{cases} R'_A = \begin{bmatrix} 1 & 0 & 0 \\ 0 & 1 & 0 \\ 0 & 0 & -1 \end{bmatrix} \text{(notate it as } I_Z) \\ R_e = \begin{bmatrix} 1-2\alpha^2 & -2\alpha\beta & -2\alpha\gamma \\ -2\alpha\beta & 1-2\beta^2 & -2\beta\gamma \\ 2\alpha\gamma & 2\beta\gamma & 2\gamma^2-1 \end{bmatrix} \end{cases}$$

Proof:
Assume $R_A = R_V \cdot K \cdot R_V{}^T$ and $J = R_V \cdot J' \cdot R_V{}^T$.
Then $K = R_e + (I-R_e) \cdot J'$ and $J' = \frac{\mathbf{t} \cdot \mathbf{n}^T}{\mathbf{n}^T \cdot \mathbf{t}}$.
Assume $\Delta R_V = R_{V_2}^T \cdot R_{V_1}$.
Then $R_{A1} = R_{A2} \Leftrightarrow \Delta R_V \cdot K \cdot \Delta R_V{}^T = K$
$\because \mathbf{n} = (\alpha, \beta, \gamma)^T$ and $\mathbf{t} = (0,1,0)^T$.
$\therefore$

$$J' = \begin{bmatrix} 0 & 0 & 0 \\ \frac{\alpha}{\beta} & 1 & \frac{\gamma}{\beta} \\ 0 & 0 & 0 \end{bmatrix}$$

Assume

$$R_e = \begin{bmatrix} r_{11} & r_{12} & r_{13} \\ r_{21} & r_{22} & r_{23} \\ r_{31} & r_{32} & r_{33} \end{bmatrix}$$

Then

$$K = \begin{bmatrix} r_{11} - \frac{\alpha}{\beta}r_{12} & 0 & r_{13} - \frac{\gamma}{\beta}r_{12} \\ r_{21} - \frac{\alpha}{\beta}(r_{22}-1) & 1 & r_{23} - \frac{\gamma}{\beta}(r_{22}-1) \\ r_{31} - \frac{\alpha}{\beta}r_{32} & 0 & r_{33} - \frac{\gamma}{\beta} \end{bmatrix} \quad (15)$$

$\because$
$\Delta R_V \cdot K \cdot \Delta R_V{}^T = K \Leftrightarrow (\Delta R_V \otimes \Delta R_V) \cdot vec(K) = vec(K)$
$\therefore vec(K)$ is the eigenvector of $\Delta R_V \otimes \Delta R_V$, and the eigenvalue is 1.
Assume the rotation axis of ΔR_V is $\delta = (0,0,1)^T$
Then the eigenvector (eigenvalue is 1) of $\Delta R_V \otimes \Delta R_V$ is

$$\begin{aligned} vec(K) = & a \begin{bmatrix} 0 & 0 & 0 & 0 & 0 & 0 & 0 & 0 & 1 \end{bmatrix}' \\ & + \frac{b}{2} \begin{bmatrix} 1 & -i & 0 & i & 1 & 0 & 0 & 0 & 0 \end{bmatrix}' \\ & + \frac{c}{2} \begin{bmatrix} 1 & i & 0 & -i & 1 & 0 & 0 & 0 & 0 \end{bmatrix}' \end{aligned} \quad (16)$$

From Eq.15 and Eq.16. We get $b = 1$ and $c = 1$.
$\therefore$

$$K = \begin{bmatrix} 1 & 0 & 0 \\ 0 & 1 & 0 \\ 0 & 0 & a \end{bmatrix} \quad (17)$$

From Eq.15 and Eq.17. We get

$$\begin{aligned} r_{11} &= 1 + \frac{\alpha}{\beta}r_{12} & r_{13} &= \frac{\gamma}{\beta}r_{12} \\ r_{21} &= \frac{\alpha}{\beta}(r_{22}-1) & r_{23} &= \frac{\gamma}{\beta}(r_{22}-1) \\ r_{31} &= \frac{\alpha}{\beta}r_{32} & r_{33} &= \frac{\gamma}{\beta}r_{32} + a \end{aligned}$$

$\therefore$

$$R_e = \begin{bmatrix} 1 + \frac{\alpha}{\beta} r_{12} & r_{12} & \frac{\gamma}{\beta} r_{12} \\ \frac{\alpha}{\beta}(r_{22} - 1) & r_{22} & \frac{\gamma}{\beta}(r_{22} - 1) \\ \frac{\alpha}{\beta} r_{32} & r_{32} & \frac{\gamma}{\beta} r_{32} + a \end{bmatrix}$$

$\because R_e$ is an orthogonal matrix
$\therefore$

$$R_e \cdot R_e{}^T = I \Rightarrow \begin{cases} r_{12} & = & \begin{cases} 0 \\ -2\alpha\beta \end{cases} \\ r_{22} & = & \begin{cases} 1 \\ 1 - 2\beta^2 \end{cases} \\ r_{32} & = & \beta(-a\gamma \pm \sqrt{a^2\gamma^2 - a^2 + 1}) \end{cases}$$

For all cases of r_{12}, r_{22} and r_{32}, with two constraints: 1) R_e is orthogonal matrix and 2) $|R_e| = 1$, we can only get two solutions

Solution 1 $\begin{cases} K & = & I \\ R_e & = & I \end{cases}$

Solution 2 $\begin{cases} K & = & I_Z \\ R_e & = & \begin{bmatrix} 1 - 2\alpha^2 & -2\alpha\beta & -2\alpha\gamma \\ -2\alpha\beta & 1 - 2\beta^2 & -2\beta\gamma \\ 2\alpha\gamma & 2\beta\gamma & 2\gamma^2 - 1 \end{bmatrix} \end{cases}$

$\because R_A = R_V \cdot K \cdot R_V^T$ and R_V's rotation axis is $\delta = (0, 0, 1)^T$
$\therefore$ This theorem is proved. $\blacksquare$

Because R'_A in solution 2 is a mirror reflection transformation about XY-plane for 3D point-cloud, it can be easily detected and restrained. So the solution 1 is the unique feasible solution and it indicates that the calibration rotation error is eliminated.

When $R_e = I$ and $\mathbf{T}_{A1} = \mathbf{T}_{A2}$, from Eq.14, we can get:

$$\Delta R_V \cdot \mathbf{T}_e = \mathbf{T}_e$$

Because the rotation axis of ΔR_V is $(0, 0, 1)^T$, the calibration translation error is eliminated on XY-plane but there is no restriction on Z-axis for $\mathbf{T}_e$. This can be solved by choosing other R_{V1} and R_{V2}, whose rotation axis is not $(0, 0, 1)^T$ to establish restriction on Z-axis for $\mathbf{T}_e$.

B. Pairwise LIDARs Calibration Theory Derivation

For the two 3D point-clouds P_t and P_r mentioned in section 4, there are two deviation transformations M_{A_t} and M_{A_r}. If P_t and P_r are aligned and each contains more than 4 non-deteriorate points, then $M_{A_t} = M_{A_r}$. As reference LIDAR calibration guarantees that $R_{e_r} = I$ and $R_{A_r} = I$, we demonstrated that if $R_{A_t} = R_{A_r} = I$, then $R_{e_t} = I$.
Proof:
Assume $J = R_V \cdot J' \cdot R_V{}^T$. Then $J' = \frac{\mathbf{t} \cdot \mathbf{n}^T}{\mathbf{n}^T \cdot \mathbf{t}}$.
$\because R_{A_t} = R_{A_r}$
$\therefore R_{e_t} + (I - R_{e_t}) \cdot J'_t = R_{e_r} + (I - R_{e_r}) \cdot J'_r$
$\therefore (I - R_{e_t}) \cdot (I - J'_t) = (I - R_{e_r}) \cdot (I - J'_r)$
When $R_{e_r} = I$, then $(I - R_{e_r}) \cdot (I - J'_r) = 0$
$\because rank(I - J'_t) = 2$ and $rank(I - R_{e_t}) = 2$ or 0,
$\therefore R_{e_t} = I$ is the only solution. $\blacksquare$
When $R_{e_t} = I$ and $\mathbf{T}_{A_t} = \mathbf{T}_{A_r}$, from Eq.14, we can get $\mathbf{T}_{e_t} = \mathbf{T}_{e_r}$, which contains error along Z-axis.

REFERENCES

[1] J. Levinson and S. Thrun, "Robust vehicle localization in urban environments using probabilistic maps." in *IEEE Int. Conf. Robotics and Automation (ICRA)*, 2010, pp. 4372–4378.

[2] S. Hu and A. Zhang, "3D laser omnimapping for 3D reconstruction of large-scale scenes," in *IEEE Urban Remote Sensing Event*, 2009, pp. 1–5.

[3] A. Segal, D. Hähnel, and S. Thrun, "Generalized-ICP." in *Robotics: Science and Systems*, J. Trinkle, Y. Matsuoka, and J. A. Castellanos, Eds. The MIT Press, 2009.

[4] B. Douillard, A. Brooks, and F. Ramos, "A 3D laser and vision based classifier," in *IEEE Intelligent Sensors, Sensor Networks and Information Processing (ISSNIP)*, 2009, pp. 295–300.

[5] F. Endres, C. Plagemann, C. Stachniss, and W. Burgard, "Unsupervised discovery of object classes from range data using latent Dirichlet allocation." in *Robotics: Science and Systems*, J. Trinkle, Y. Matsuoka, and J. A. Castellanos, Eds. The MIT Press, 2009.

[6] K. Lai and D. Fox, "3D laser scan classification using web data and domain adaptation." in *Robotics: Science and Systems*, J. Trinkle, Y. Matsuoka, and J. A. Castellanos, Eds. The MIT Press, 2009.

[7] J. Guivant, E. Nebot, and S. Baiker, "Autonomous navigation and map building using laser range sensors in outdoor applications," *Int. J. Robotic Systems*, vol. 17, no. 10, pp. 565–583, 2000.

[8] A. Kelly, "An intelligent predictive control approach to the high-speed cross-country autonomous navigation problem," Ph.D. dissertation, Robotics Institute, Carnegie Mellon University, 1995.

[9] S. Thrun, M. Montemerlo, H. Dahlkamp, D. Stavens, A. Aron, J. Diebel, P. Fong, J. Gale, M. Halpenny, G. Hoffmann *et al.*, "Stanley: The robot that won the darpa grand challenge," *Int. J. Field Robotics*, vol. 23, no. 9, pp. 661–692, 2006.

[10] J. Underwood, "Reliable and safe autonomy for ground vehicles in unstructured environments," Ph.D. dissertation, University of Sydney, 2009.

[11] D. Scaramuzza, A. Harati, and R. Siegwart, "Extrinsic self calibration of a camera and a 3D laser range finder from natural scenes." in *IEEE/RSJ Int. Conf. Intelligent Robots and Systems (IROS)*, 2007, pp. 4164–4169.

[12] G. Lisca, P. Jeong, and S. Nedevschi, "Automatic one step extrinsic calibration of a multi layer laser scanner relative to a stereo camera," in *IEEE Int. Conf. Intelligent Computer Communication and Processing (ICCP)*, 2010, pp. 223–230.

[13] Q. Zhang and R. Pless, "Extrinsic calibration of a camera and laser range finder (improves camera calibration)." in *IEEE/RSJ Int. Conf. Intelligent Robots and Systems (IROS)*, 2004, pp. 2301–2306.

[14] J. P. Underwood, A. Hill, T. Peynot, and S. Scheding, "Error modeling and calibration of exteroceptive sensors for accurate mapping applications." *J. Field Robotics*, vol. 27, no. 1, pp. 2–20, 2010.

[15] C. Gao and J. R. Spletzer, "On-line calibration of multiple LIDARs on a mobile vehicle platform." in *IEEE Int. Conf. Robotics and Automation (ICRA)*, 2010, pp. 279–284.

[16] M. Sheehan, A. Harrison, and P. Newman, "Self-calibration for a 3D laser," *Int. J. Robotics Research*, vol. 31, no. 5, pp. 675–687, 2012.

[17] J. P. Underwood, A. J. Hill, and S. Scheding, "Calibration of range sensor pose on mobile platforms." in *IEEE/RSJ Int. Conf. Intelligent Robots and Systems (IROS)*, 2007, pp. 3866–3871.

[18] R. Unnikrishnan and M. Hebert, "Fast extrinsic calibration of a laser rangefinder to a camera," Robotics Institute, Tech. Rep. CMU-RI-TR-05-09, 2005.

[19] O. Jokinen, "Self-calibration of a light striping system by matching multiple 3-D profile maps," in *IEEE 3-D Digital Imaging and Modeling*, 1999, pp. 180–190.

[20] J. Levinson and S. Thrun, "Unsupervised calibration for multi-beam lasers," in *International Symposium on Experimental Robotics*, 2010.

[21] M. He, H. Zhao, F. Davoine, J. Cui, and H. Zha, "Pairwise LIDAR Calibration Using Multi-Type 3D Geometric Features in Natural Scene ," in *IEEE/RSJ Int. Conf. Intelligent Robots and Systems (IROS)*, 2013.